JACS
JOURNAL OF THE AMERICAN CHEMICAL SOCIETY
Article
pubs.acs.org/JACS

Discovery of a Phosphor for Light Emitting Diode Applications and Its Structural Determination, $Ba(Si,Al)_5(O,N)_8:Eu^{2+}$

Woon Bae Park,[†] Satendra Pal Singh,[†] and Kee-Sun Sohn*

Faculty of Nanotechnology and Advanced Materials Engineering, Sejong University, Seoul 143-747, Korea

Supporting Information

ABSTRACT: Most of the novel phosphors that appear in the literature are either a variant of well-known materials or a hybrid material consisting of well-known materials. This situation has actually led to intellectual property (IP) complications in industry and several lawsuits have been the result. Therefore, the definition of a novel phosphor for use in light-emitting diodes should be clarified. A recent trend in phosphor-related IP applications has been to focus on the novel crystallographic structure, so that a slight composition variance and/or the hybrid of a well-known material would not qualify from either a scientific or an industrial point of view. In our previous studies, we employed a systematic materials discovery strategy combining heuristics optimization and a high-throughput process to secure the discovery of genuinely novel and brilliant phosphors that would be immediately ready for use in light emitting diodes. Despite such an achievement, this strategy requires further refinement to prove its versatility under any circumstance. To accomplish such demands, we improved our discovery strategy by incorporating an elitism-involved nondominated sorting genetic algorithm (NSGA-II) that would guarantee the discovery of truly novel phosphors in the present investigation. Using the improved discovery strategy, we discovered an Eu^{2+}-doped AB_5X_8 (A = Sr or Ba, B = Si and Al, X = O and N) phosphor in an orthorhombic structure ($A2_1am$) with lattice parameters a = 9.48461(3) Å, b = 13.47194(6) Å, c = 5.77323(2) Å, $\alpha = \beta = \gamma = 90°$, which cannot be found in any of the existing inorganic compound databases.

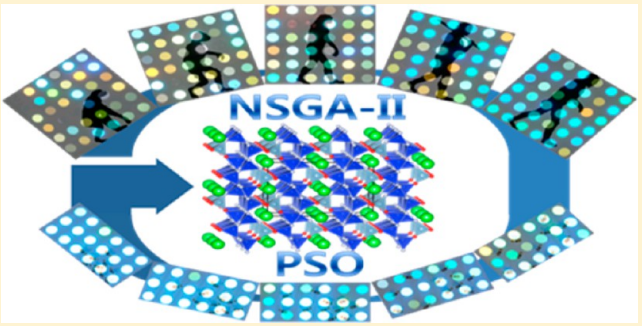

1. INTRODUCTION

In the research area of inorganic luminescent materials (phosphors), the novelty of materials is a controversial issue relative to qualities such as crystallographic structure, chemical composition, and functionality. Many of the materials that may be referred to as novel do not seem to be novel in any real sense. These uncertainties have actually led to intellectual property (IP) complications in industry, and several lawsuits have been the result.[1−3] Therefore, we want to clarify exactly what is meant by the term "novel" in the field of academics to provide the field of industry with a foundation on which IP-availability issues can be clarified. As mentioned in our previous report,[4,5] a primary criterion on which we judge the novelty of a phosphor (in particular, for use in light emitting diode (LED) applications) is the crystallographic structure rather than the composition. In addition, either the creation of a novel function or an improvement in an existing function is the second primary criterion that proves the "novelty" of a discovered phosphor. Therefore, neither a slight variation[6] nor a hybrid[7] of a well-known phosphor would be considered an IP-available novel material. For instance, a slight composition change induced by substitution or doping would no longer take effect, if the crystallographic structure and the functionality were unaltered. This has recently been clarified in courts of law.[3] Based on the reasonable definition of novelty for phosphor materials, we want to develop a greater number of novel phosphors for use in LED applications.

Our goal was to discover IP complication-free novel phosphors in the present investigation. In our previous report,[4] we suggested a systematic materials discovery strategy that combines heuristics optimization with high-throughput experimentation (HTE) to discover IP complication-free novel phosphors for use in LEDs. In particular, nondominated sorting genetic algorithm (NSGA)[8] and particle-swarm optimization (PSO)[9] were used for the discovery process along with solid-state HTE. More importantly, it is pragmatic to parametrize the novelty of materials so as to avoid futile efforts aimed at the discovery of existing phosphors, but rather to pursue genuine novelty during the discovery process.

In the present investigation, we proposed an improved discovery strategy compensating for the weak points of the previously reported strategy.[4] An elitism-involved NSGA, called NSGA-II, was more recently developed to considerably reduce the complexity.[10] In NSGA-II, two subsequent generations are combined to find the nondominated solutions. Because our heuristics optimization process, such as NAGA-II and PSO, was based on the experimental evaluation of objective function by

Received: September 30, 2013
Published: January 17, 2014

   dx.doi.org/10.1021/ja409865c | J. Am. Chem. Soc. 2014, 136, 2363−2373

Table 1. Categorization of Well-Known LED Phosphors

type	description of definition and comments	basic chemical formula (typical title)
Type I	These phosphors are very well-known and were used in old-fashioned applications even before the advent of blue (or NUV) LEDs. As a result of wide screening and data mining implemented among those well-known existing phosphors at the point of the blue (or NUV) LED invention, only a few phosphors of this type were pinpointed. The YAG phosphor is an example of a Type I phosphor. It is our opinion that no more Type I phosphors are being developed because the tests for possible use in LEDs have already been completed for almost all existing phosphors.	$Y_3Al_5O_{12}:Ce^{3+}$ (YAG); $Sr_2SiO_4:Eu^{2+}$ (orthosilicate)
Type II	These phosphors can be created by a slight modification of well-known LED phosphors. Either substitution or codoping has been applied to many already well-established LED phosphors to discover IP-independent novel phosphors. TAG used to be an example of Type II. It was definitely effective to pursue Type II in the past at the relatively early stage of LED development, as shown in the case of TAG and LuAG. Afterward, recent IP claims not only on the composition but more importantly on the structure and thereby every original IP involves most of the possible compositions in a fixed-claimed structure. As long as the original IP had a main claim on the structure, the Type II approach might bring about IP conflicts by referring to the results of recent lawsuits. It should be noted that we do not deny the scientific merit induced by the Type II approach; only the usefulness of Type II phosphors in industry is in question. A variety of Type II approaches, e.g., solid solution, codoping, and hybridization are highly recommended for scientific purposes.	$Ln_3A_5O_{12}:Ce^{3+}$, Ln = Tb, Lu; A = Al, Ga, etc. (TAG, LUAG); $Ae_2SiO_4:Eu^{2+}$, Ae = Sr, Ba, Mg, Ca, etc. (BOSE); $AeAlSiX_3:Eu^{2+}$, Ae = Sr, Ca; X = N, O, C, F, Cl, etc. (SCASN). Infinite numbers of possible Type II phosphors are available based on all of Type I, III, and IV phosphors
Type III	The structure of the host materials of these phosphors was very well-known and easily found in conventional crystallographic databases. However, the activator incorporation (so-called phosphorization) had never been implemented. In other words, Type III first exists as something different but becomes a phosphor because of activation (activator doping). It is not coincidental that most prestigious, commercially available LED phosphors belong to Type III, because they have a relatively long history with the best synthesis, reliability and integrity during a relatively long period of time prior to becoming a phosphor. If novel phosphors of this type are discovered, there would be no IP complications.	$M\text{-}(Si,Al)_3(N,O)_4:Eu^{2+}$, M = Ca, Li, Y, etc. ($\alpha$, β-SIALON); $CaAlSiN_3:Eu^{2+}$ (CASN); $La_3Si_6N_{11}:Ce^{3+}$ (LASN); *$SrSi_2O_2N_2:Eu^{2+}$ (SION or 1222). *The indexing result was reported without exact structure refinement in 1994,[14] and Eu^{2+} doping made it a phosphor for LED in 2005.[15] However, more reliable structure was very recently refined and reported in 2013.[16]
Type IV	These phosphors are real novel phosphors developed for the purpose of their use for LED applications. In other words, Type IV phosphors are born as a phosphor for use in LEDs. The structure should be determined by discovery in order to confirm that it is not an elemental substitution of well-known materials (or phosphors) that already exist in the crystallographic database. Unfortunately, the performance of Type IV phosphors at the current stage is not as good as Type III phosphors, and it should also be noted that some Type IV were withdrawn soon after they became available on the market because of insufficient performance. There is no doubt that novel phosphors of this type would cause no IP complications.	*$(Sr,Ba)_2Si_5N_8:Eu^{2+}$ (258); $SrAlSi_4N_7:Eu^{2+}$; $Ba_3Si_6O_{12}N_2:Eu^{2+}$ (BUSON); $La_{4-x}Ca_xSi_{12}O_{3+x}N_{18-x}:Eu^{2+}$ (LCSON). *The structure of the host was discovered prior to the phosphorization but it was categorized into Type IV because both the discovery of the host and the phosphorization were achieved by the same group.[23]

the assistance of HTE, it is impossible to run as many iterations as a conventional computation-only problem usually runs. However, our optimization task allowed for only a few iterations because of the limited cost and time. The final goal of NSGA-II in the present investigation was not to achieve complete optimization but rather to find hints to chart a rough path toward optimization. Therefore, the use of NSGA-II was a great help in the discovery of novel phosphors at a relatively early stage of development.

In previous reports, we detailed the discovery of commercially interesting materials such as $La_{4-x}Ca_xSi_{24}O_{3+x}N_{18-x}:Eu^{2+}$, $Ce_{4-x}Ca_xSi_{24}O_{3+x}N_{18-x}:Eu^{2+}$, $Ba_{1.5}Ca_{0.5}Si_5N_6O_3:Eu^{2+}$, and $Ca_{15}Si_{20}N_{30}O_{10}:Eu^{2+}$.[4,11−13] $La_{4-x}Ca_xSi_{24}O_{3+x}N_{18-x}:Eu^{2+}$ and $Ce_{4-x}Ca_xSi_{24}O_{3+x}N_{18-x}:Eu^{2+}$ are now being considered for commercialization in the field. That report[4] lacked material details, and was focused more on the discovery strategy. The present report was focused more on the discovered material. We discovered outstanding, novel phosphors for use in LEDs in the present investigation: $Sr(Si,Al)_5(O,N)_8:Eu^{2+}$ and $Ba(Si,Al)_5(O,N)_8:Eu^{2+}$. The material details, including the structural determination process, were discussed more extensively in the present investigation. The structure of both $Sr(Si,Al)_5(O,N)_8:Eu^{2+}$ and $Ba(Si,Al)_5(O,N)_8:Eu^{2+}$ was found to be orthorhombic in an $A2_1am$ space group with identical atomic arrangements, but with a slightly different lattice size. We focused only on $Ba(Si,Al)_5(O,N)_8:Eu^{2+}$ because it surpassed $Sr(Si,Al)_5(O,N)_8:Eu^{2+}$ in terms of luminescent properties. Therefore, a detailed structural determination and photoluminescence (PL) property examination of $Ba(Si,Al)_5(O,N)_8:Eu^{2+}$ are presented here, but those for $Sr(Si,Al)_5(O,N)_8:Eu^{2+}$ were skipped. Along with the major discovery, a minor discovery was accomplished in the present approach with published details to follow soon. All the novel phosphors discovered in the present investigation do not exist in any of the existing structural databases, and therefore, these are completely free of IP complications. Accordingly, $Ba(Si,Al)_5(O,N)_8:Eu^{2+}$ and their binary solid solutions could soon be used in UV LED applications such as displays and lighting operations.

2. EXPERIMENTAL PROCEDURES

The commercially available starting powder materials, CaO (Kojundo, 99.9% UP), SrO (Kojundo, 98%), BaO (Kojundo, 99% UP), $SrCO_3$ (Kojundo, 98%), $BaCO_3$ (Kojundo, 99% UP), Al_2O_3 (Kojundo, 99.99%), AlN (Kojundo, 99.9%), α-Si_3N_4 (Aldrich, unreported), α-Si_3N_4 (Ube, unreported), and Eu_2O_3 (Kojundo, 99.9%), were dispensed into a so-called combi-chem container, a specially designed sample container made of BN ($80 \times 40 \times 20$ mm^3), which involved 18 sample sites that were 8.5 mm in diameter and 16 mm in depth. Preparations such as mixing, grinding, and firing of a large number of samples were executed inside the combi-chem container. The total amount of raw materials at each sample site was about 0.3 g, which produced a sufficient amount of final phosphor powder available for use in any of the conventional characterizations. The exact amounts of the raw materials were weighed and dispensed automatically to the sample sites using a powder-extruder system in a high-throughput manner with a robotic platform (Swave, ChemSpeed Tech Co., Ltd.). The mixing and grinding was executed by vibrating the combi-chem containers with pins inserted inside the sample sites. Since the automatic mixing and grinding turned out to be unsatisfactory, we prepared 36 agate mortars with an inside diameter of 450 mm, and the samples were transferred to these agate mortars and further ground manually. Although this manual process required much time, the final quality of the samples was improved significantly. The mixed raw materials were retransferred to the combi-chem container and then

dx.doi.org/10.1021/ja409865c | J. Am. Chem. Soc. 2014, 136, 2363−2373

fired at 1600 °C for 4−8 h under a N_2 gas flow (500 mL/min) in a sealed tube furnace. Two combi-chem containers (i.e., 36 samples) were fired simultaneously.

Each fired sample was ground and subjected to X-ray diffraction (XRD) and PL analysis. The emission spectra were monitored at either 400 or 460 nm excitation in a pseudohigh-throughput manner using an in-house-fabricated continuous-wave (CW) PL system equipped with a xenon lamp. Finally, discovered novel samples were examined using synchrotron radiation X-ray diffraction (SR-XRD). The SR-XRD measurements of the selected sample were conducted using the 9B high-resolution powder-diffraction beamline at the Pohang Accelerator Laboratory (PAL). The incident synchrotron X-rays were monochromatized to a wavelength of 1.5472 Å by a double-bounce Si(111) monochromator and calibrated with a SRM660a standard sample. The detector arm of the diffractometer had soller slits with an angular resolution of 2°, a flat Ge{111} crystal analyzer, an antiscatter baffle, and a scintillation detector. Data were collected in the angular 2θ range of 10.0°−130.5° with a step size of 0.005°.

3. NOVELTY OF LED PHOSPHORS

Many reports have alleged the discovery of novel phosphors. However, it is our opinion that most of these phosphors do not meet the requirements for the term novel. Prior to in-depth discussions regarding the discovery process of novel phosphors, the definition of a novel phosphor should be clarified. First, the definition should be thoroughly based on science, but there must also be a focus on the issue of whether or not IP complications will occur. For convenience, we have categorized the current well-known LED phosphors into four different types.[4] To clarify for readers, we reinforced the explanation on the philosophy behind this categorization, as shown in Table 1 along with reinforced examples.

There is no doubt that either Type III or Type IV should be the only option that we have to pursue from both a scientific and a practical point of view if the novelty of discovered phosphors are a concern. To preclude some controversies relative to Type II phosphors, we must clarify the criterion on which we can judge whether the structures of concern are identical. We referred to a recent report by Allmann and Hinek[17] regarding this issue. They argued that two crystal structures are regarded as isostructural if they are isoconfigurational. So, the same structure we mentioned in constructing our phosphor categorization was thoroughly based on the criterion put forth by Allmann and Hinek.[17] For a more pragmatic understanding of our categorization, an extreme example is introduced and discussed below. Chiu et al.[18] and Wang et al.[19] recently reported novel phosphors $Ca_3Si_2O_4N_2$:Eu^{2+} and $Sr_3Si_2O_4N_2$:Eu^{2+}, which showed green and red light emissions at 380 and 460 nm excitations, respectively. It is not possible to find this phosphor in any of the crystallographic databases. However, this phosphor does not seem to be a Type IV, because they refined the structure of these phosphors using the well-known $Ca_3Al_2O_6$ and $Ba_3Ga_2O_6$ structure ($Pa3$ space group).[20,21] This means that these phosphors are nothing but the partly substituted composition of a well-known compound, the structure of which has been well-defined and available in the structural database. Moreover, $Sr_3Al_2O_6$, the structure of which is identical to that of $Ca_3Al_2O_6$ and $Ba_3Ga_2O_6$, has been used as a phosphor host by Eu^{2+} activation, so that it constituted a red phosphor. Consequently, both $Ca_3Si_2O_4N_2$:Eu^{2+} and $Sr_3Si_2O_4N_2$:Eu^{2+} are Type II phosphors that are based on a strict judgment. From a practical point of view, however, these might not give rise to IP complications because $Sr_3Al_2O_6$:Eu^{2+} has never been regarded as a good candidate for a LED phosphor, and a well-established IP for $Sr_3Al_2O_6$:Eu^{2+} has never been published.

Our goal in the present investigation was not to either improve or modify the luminescent properties by adopting Type II approaches, but rather it was to pinpoint novel Type III and Type IV phosphors. Such an effort should deserve more credit and appreciation in contrast to conventional Type II clichés. As was described in Table 1, the Type III novel phosphors would be most promising if they could be discovered. However, the probability of discovering novel Type III phosphors is diminishing because over the past decade many members of the phosphor industry and academic groups have pursued the discovery of Type III phosphors by ransacking all of the existing structural databases and attempting to synthesize all plausible candidates, a practice that is ongoing. In this context, we intended to pursue Type IV rather than Type III in the present investigation and thoroughly avoided following Type II. It should be noted that we never denigrated the scientific importance of the Type II approach, and we respect some of the brilliant improvements that have been acquired by modifying the composition while the structure remains unvaried.[22] It is our opinion that such a brilliant achievement by using the Type II approach may have great scientific merit, but that it might be of no use from a practical point of view, which means that a related industry would not welcome Type II phosphors due to their potential risk in association with IP complications.

4. RESULTS AND DISCUSSION

4.1. Discovery Strategy and Discovery Process of Novel Phosphors. The heuristics optimization-involved phosphor discovery process adopted in our previous investigation was modified in the present investigation. The modification was focused on the preliminary rough screening process based on a nondominated sorting genetic algorithm (NSGA). While we had used a standard NSGA in the previous report,[4] the present investigation adopted an improved version of the NSGA, namely, an elitism-involved NSGA, the so-called NSGA-II.[10] The effect of this modification on the discovery process was not easy to detect for those who are unfamiliar with the use of a NSGA. However, there clearly was a faster increase in the number of samples with a higher structural rank and PL intensity compared with the previous case. With the exception of this modification in the preliminary screening process, all the other processes were analogous to the previous case, wherein we employed a structural rank, which is indicative of the novelty of materials as evaluated from the XRD data. Particle swarm optimization (PSO) was used for the ensuing composition to fine-tune the process in order to pinpoint the best processing composition. The details of heuristics optimization and the structural rank are aptly described in the Supporting Information (Table S2). Rather than details of the methodology, the present investigation was focused more on the discovered material.

The discovery process was executed in a relatively small composition space while the processing condition was fixed. One might argue that the synthesis conditions, such as thermal history and atmosphere control, would be more important than the starting composition (or processing composition) in terms of whether or not a novel compound can be claimed. We totally agree with this argument. In this context, we began by implementing the PSO for three different processing conditions.[5] However, we adopted a fixed processing condition

in the present investigation. Prior to the determination of processing conditions, we considered them in conjunction with the processing composition space. If the space was well-defined and sufficiently narrow, then a single processing condition would suffice. We have consistently argued that our combinatorial materials discovery was not designed to introduce impractical luminescent materials out of a huge number of arbitrarily chosen composition spaces even including many materials with no luminescence, but rather, to pinpoint promising phosphors that would be immediately useful, out of a plausible, reduced composition space where all materials exhibit a certain level of luminescence. Rather than a conventional approach to combinatorial materials science, our approach should be considered a sort of pragmatic materials discovery that focuses more on the needs of industry. In this regard, the processing composition space, wherein our heuristics optimization-involved discovery process was executed, was designed very carefully by taking discovery potential and current industry needs into account, as shown in Figure 1. As a result, we were able to significantly narrow the composition search space enough to establish the processing condition.

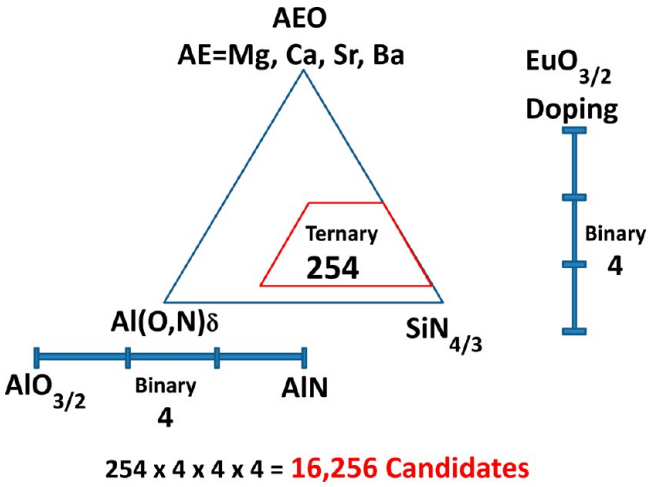

Figure 1. Design of decision parameter space (phosphor composition search space) for NSGACMS.

The composition space that we adopted in the present investigation consisted of eight elements: MgO, CaO, SrO, BaO, Eu_2O_3, Al_2O_3, AlN, and Si_3N_4. These eight starting materials would constitute an infinite size of composition space. Such a huge composition space could never be undertaken as a decision parameter space for our heuristics optimization-involved discovery process, because our heuristics optimization process was not a computation-only process but was an experiment-oriented process involving the experimental evaluation of objective function. This means that several hundred phosphor samples were actually synthesized and characterized in the heuristics optimization process. Accordingly, the size of the composition space should be reduced significantly so as to alleviate experimental burdens and costs, that is, to reduce the number of phosphor samples that must be tested. First, we reduced the major ternary space (consisting of alkali earth oxide-aluminum precursor (oxide or nitride)-silicon nitride) to a small area in the vicinity of the Si_3N_4 side. The philosophy behind this reduction process was backed up by actual preliminary synthesis experimentation, and not just by intuition. In fact, most of the compositions outside of this downsized area were melted down at temperatures above 1600 °C, and the area close to the (AlN, Al_2O_3)-Si_3N_4 binary composition just underneath our reduced composition area led only to well-known SIALON phosphors. It is obvious that every sample in the reduced composition space gave a powder form exhibiting a certain level of Eu^{2+} luminescence. Our primary task was to pinpoint either Type III or Type IV novel phosphors with an acceptable luminescence among those in the reduced composition space, as shown in Figure 1.

We never allowed for the mixture of the four alkali earth elements in the reduced composition space. It should be noted that the novel structure of discovery for Type III and Type IV was our main goal rather than just the discovery of high-luminescence materials. Once a novel structure was formulated based on a single alkali earth element, the probability of constituting other novel structures by adopting a small amount of other alkali earth elements as substituents, should have been very low. Instead, alkali earth element substitution should play a significant role only in improving the luminescent properties such as luminance and color control, while the structure remains unvaried. Although the alkali earth mixture could result in promising solid-solution types of single-phase phosphors with improved luminescent properties, such a solid solution approach was not employed during the discovery process, because it can be executed separately after the discovery process.

Another issue regarding the reduction of composition space was to simplify the Al_2O_3−AlN binary composition and also the Eu^{2+} content. In fact, we fine-divided neither the Al_2O_3−AlN binary composition nor the Eu^{2+} content. They were simply divided into only 4 steps, which was sufficient to differentiate their effect. It was also noted that it was of no use to fine-divide the selected range of the Al_2O_3−AlN binary composition and the Eu^{2+} content because the entire selected range was also reasonable and narrow enough, which was based on experience and knowledge. Despite such a severe reduction in the search space, we still had a total of 16,256 different compositions in our reduced space. This number was impossible to screen based on a one-by-one strategy. Even when using our solid-state HTE-based powder process, it was still very difficult to track down all of them. Also, it definitely was not necessary to screen all of the 16,256 candidates. Therefore, we needed the heuristics optimization-involved discovery process.

Figure 2 shows the results from the NSGA-II-involved combinatorial material search (NSGACMS) process, which is a preliminary, rough screening process for phosphor discovery. NSGACMS was iterated through five consecutive generations. Each generation contained 36 phosphor samples, the PL intensity and structural rank of which were evaluated based on HTE, and were classified according to the Pareto optimality theory[8] and plotted with the same Pareto group interconnected, as shown by the gray lines in Figure 2. The definition of structural rank is aptly described in the Supporting Information. This shows that a higher structural rank is indicative of a greater portion of unknown phases in the sample. It is obvious that the number of high-rank samples in Figure 2 continued to increase as the NSGACMS process approached later generations. The first generation was randomly chosen but included many well-known phases, some of which were well-known phosphors. Table S4 lists the processing composition, the constituting phases, the structural rank, and the PL intensity for all samples appearing from the first to the fifth generation in the NSGACMS process. The constituting phase summary was of

dx.doi.org/10.1021/ja409865c | J. Am. Chem. Soc. 2014, 136, 2363−2373

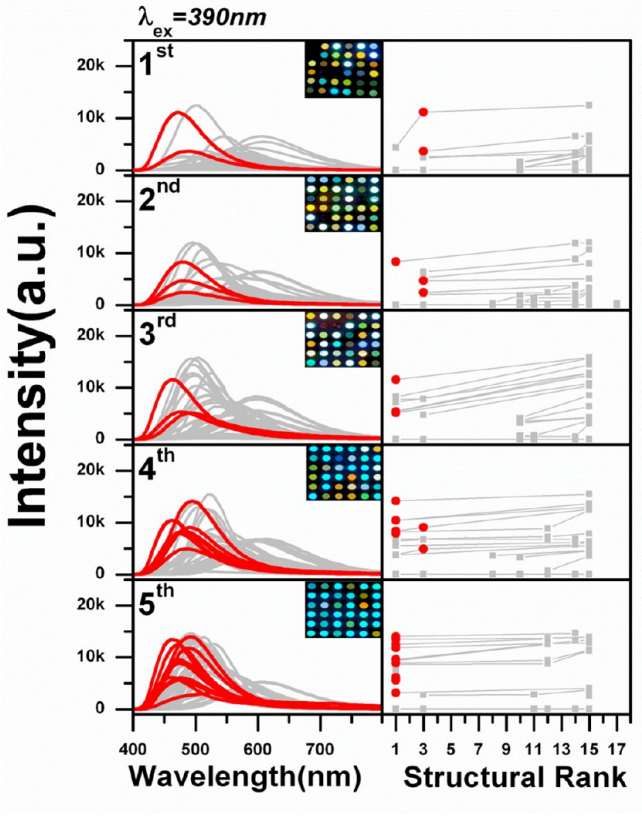

Figure 2. The NSGACMS-execution results: plot of PL intensity versus structural rank for each generation, the so-called Pareto plot, along with emission spectra at 390 nm excitation and actual sample photos taken under a 365 nm UV lamp. The composition, PL-intensity, structural-rank and phase-identification data are shown in Table S4.

particular concern because it was used for the determination of structural rank for every sample. We took into account two major phases only from each XRD pattern in determining the structural rank, while the other minor phases were ignored. Besides well-known phases, we also detected several unknown phases in the first generation, but these were all mixed with some other impurity phases. Particular concern was focused on an unknown phase, which was referred to as Unknown1, the emission light of which was blue. Unknown1 is designated as a red dot in Figure 2, and its corresponding spectrum is highlighted in red. The composition is also marked in red in Table S4. Actual photos for each generation taken at a 365 nm excitation are included as insets in Figure 2. Our task at this preliminary screening step was not to identify all the unknown phases, including Unknown1, on a one-by-one basis but to drive the NSGACMS process to end up with one certain unknown single phase by minimizing impurities and thereby to secure the novelty of the phosphor. In fact, such an evolution to an unknown single phase with an acceptable luminescence took place as the NSGACMS process proceeded to the fifth generation. The number of red marks corresponding to Unknown1 increased significantly as the evolution graduated to later generations. The tentative optimization up to the fifth generation appeared to converge around Unknown1 rather than around any other unknowns. The number of red dots and red spectra gradually increased, as shown in Figure 2. The actual photo in the inset of Figure 2 showed that although there were some other color emissions as well as nonluminescent samples in the early generations, the fifth generation was full of the blue emissions from Unknown1 phosphors. An interesting point is that there was no human intervention during this evolutionary discovery process; the NSGA-II organized the entire process.

It is customary for conventional NSGA-II computation to iterate for thousands of times until a complete optimization is achieved. On the contrary, our NSGACMS process was finished after only the fifth generation because we adopted the experimental evaluation of objective functions. However, such a limited iteration can be rationalized by the fact that the most dramatic improvement is always achieved at the initial stage of iterations regardless of the heuristics-based optimization algorithms that are employed. Another rationale supporting the limited number of iterations in our NSGACMS process is that further optimization was obtained by another heuristics optimization strategy in a more reduced composition space. The main goal of the NSGACMS process was not to achieve a final convergence on the global optimum but to provide early information to direct the ensuing fine-tuning of the process in a promising direction. Accordingly, the NSGACMS process enabled us to efficiently reduce the search space in the ensuing fine-tuning process. In this context, instead of going further to later generations in the NSGACMS process, we scrutinized the results from the NSGACMS process, as shown in Table S4. Such scrutiny led to an interesting result whereby the NSGA process ended up with an unknown phase (Unknown1). Although we discovered this interesting unknown phase in the NSGACMS process, further refinement in phase purity and a higher PL intensity were definitely required. Therefore, we reduced further the composition search space around the Unknown1 compositions and then executed a fine-tuning process in this further-reduced search space.

A PSO-involved combinatorial material search (PSOCMS) process was employed for the fine-tuning process following the NSGACMS process. Whereas a discrete search space was used for the NSGACMS process, the fine-tuning process was executed in a continuous search space. It is accepted that a PSO has a greater advantage in the continuous parameter search space,[7] so that our choice of a PSO for the ensuing fine-tuning was reasonable. First, the processing composition search space was dramatically reduced for the PSOCMS process. We noticed that the Unknown1 phase was composed of BaO (or SrO), Al_2O_3, and Si_3N_4. Two ternary host composition search spaces were reconstructed for use in the PSOCMS process, as shown at the top of Figure 3, one for $BaCO_3$−Al_2O_3−Si_3N_4 and the other for $SrCO_3$−Al_2O_3−Si_3N_4. The ternary composition space was truncated, such that the actual space was further reduced toward the Si_3N_4 corner. In addition to this ternary composition, the Eu^{2+} activator concentration range was also incorporated in the search space, and thereby we constructed a prismlike composition search space, wherein the PSOCMS process was iterated. It should be noted that we changed the Ba (and Sr) precursor from simple oxide to carbonate in the PSOCMS process, since we confirmed that the carbonate precursor was better in terms of the luminescent and structural properties of the Unknown1 phase.

Only the PL intensity was used as an objective function in the PSOCMS process. We excluded any structural property-related objective function in the PSOCMS process, because the second reduced search space was sufficiently small and thereby the structures of a majority of the samples in this search space did not deviate from the Unknown1 structure. In addition, the

dx.doi.org/10.1021/ja409865c | J. Am. Chem. Soc. 2014, 136, 2363−2373

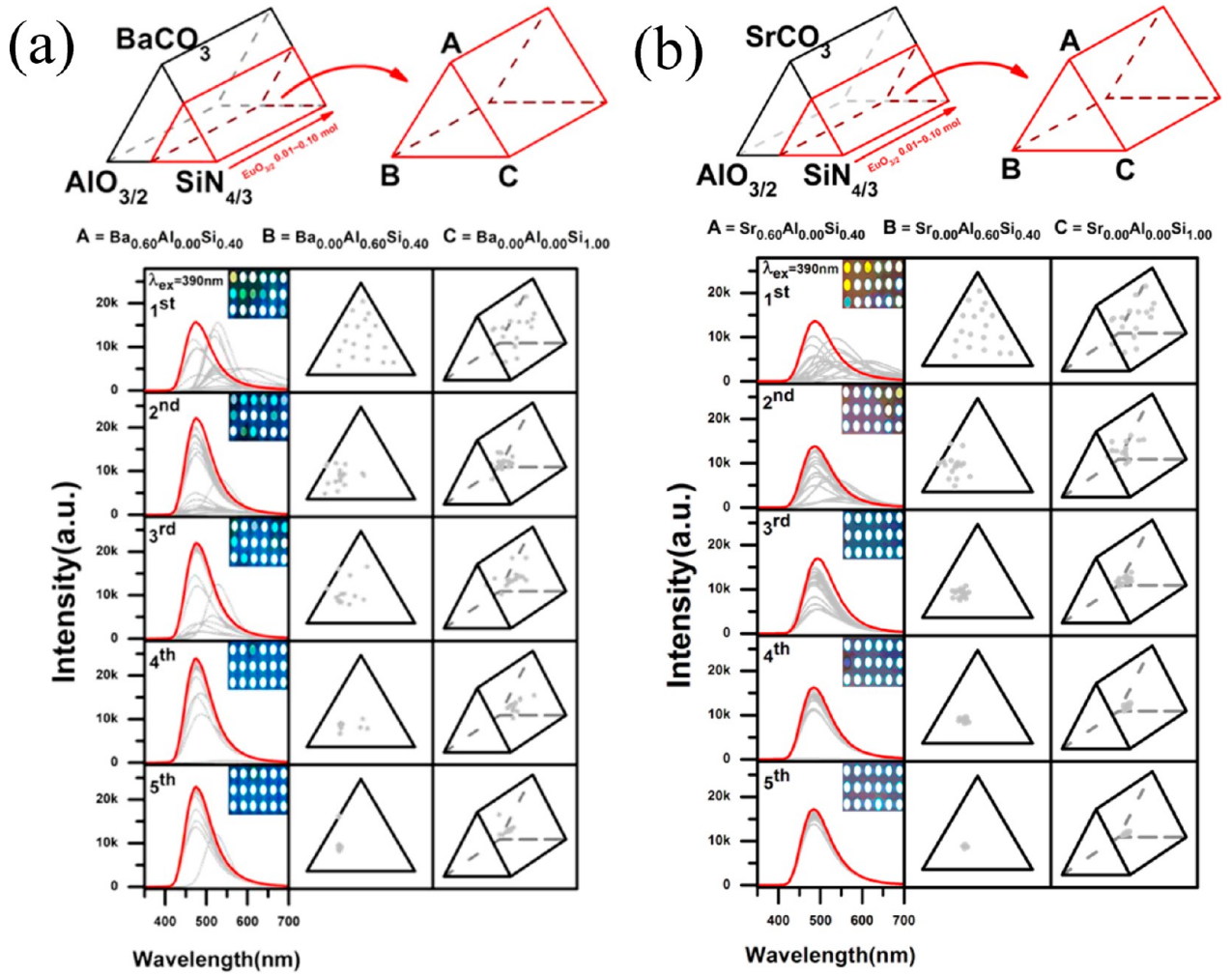

Figure 3. PSOCMS-execution results: instantaneous swarm positions in quaternary composition space to the fifth swarm, showing a rapid convergence to an optimum point (a) for $BaCO_3$–Al_2O_3–Si_3N_4–Eu_2O_3 and (b) for $SrCO_3$–Al_2O_3–Si_3N_4–Eu_2O_3. The Eu^{2+} activator concentration ranged from 0 to 10 mol %. The ternary $BaCO_3$ (or $SrCO_3$)–Al_2O_3–Si_3N_4 composition space is also presented for better understanding of the host compositions. The composition data along with the PL intensity are provided in Table S5.

structure of Ba- and Sr-based Unknown1 phases appeared to be identical because their XRD patterns were identical. Five consecutive swarms are presented in Figure 3. The first swarm shows randomly distributed samples in the search space, and they gradually flocked onto a promising area in later swarms. The composition and PL intensity of all samples appearing during the PSOCMS process are listed in Table S5. The spectrum of the best sample of each swarm is highlighted in red in Figure 3, and their composition is highlighted in red in Table S5. The highest and average PL intensities of each swarm kept increasing as the swarm evolved. The best composition, which was the converged point in the search space, was reached at the fifth swarm. Although the highest PL intensity was elicited from the fourth swarm rather than from the fifth, in the case of the $BaCO_3$–Al_2O_3–Si_3N_4 system such a small discrepancy due to experimental inconsistency was acceptable. The Ba-based Unknown1 phase seemed more promising than the Sr-based Unknown1 phase in terms of phase purity and PL intensity. The structural identification (determination) of the Unknown1 phase will be described in detail in the following subsection. It should be noted that the Unknown1 phase was definitely categorized as a Type IV, which should be free from any IP complications. The PL and PLE spectra are shown in Figure 4,

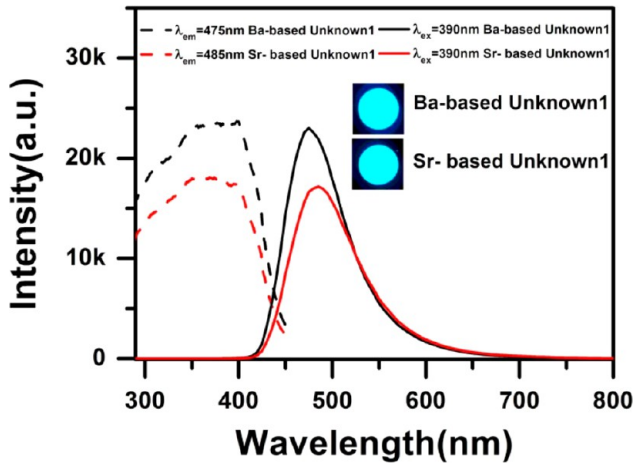

Figure 4. Emission and excitation spectra of Unknown1 phosphors, which turned out to be $Ba(Si,Al)_5(O,N)_8:Eu^{2+}$ and $Sr(Si,Al)_5(O,N)_8:Eu^{2+}$.

exhibiting a band-type emission based on a typical 5d–4f transition. The emission peak location was at 475 and 485 nm for Ba- and Sr-based Unknown1, respectively. The excitation

dx.doi.org/10.1021/ja409865c | J. Am. Chem. Soc. 2014, 136, 2363–2373

band at around 390 nm in the PLE spectrum indicates that these phosphors can be used for NUV LED chip-based applications.

Besides the Unknown1 phase, we also observed several more unknown phases during the NSGACMS process. Among those minor unknowns, we were more interested specifically in the reddish-yellow light-emitting ones. The emission spectrum of these peaked at around 600−630 nm. All of this type of spectra belongs to the reddish-yellow light-emitting unknown phase. Although the luminescent intensity was not promising, the emission and excitation properties were more suited to blue LED chip applications. In this regard, we also implemented another PSOCMS that targeted this phase, as shown in Figure S3 in the Supporting Information. The reduced composition search space in this case was similar to those used for the Unknown1 phase. However, it was a lot smaller than those used for the Unknown1 phase. Accordingly, the emissions from the Unknown1 phases were observed in the randomly chosen first swarm but they soon disappeared and thereby the last (fifth) swarm was wholly composed of the reddish-yellow light-emitting unknown phase. The ensuing phase identification was ongoing but it was not as easy as in the Unknown1 case because of the observation of a greater number of impurity phases along with the main unknown phase. It will take some time to identify the exact structure of this novel reddish-yellow light-emitting phosphor candidate, but the results will be reported soon.

4.2. The Structural Determination of Unknown1. To determine the crystal structure of the Ba- and Sr-based Unknown1 phases, we first concentrated on the Ba-based Unknown1 phase because of its excellence in luminescent properties as compared to the Sr-based Unknown1 phase. We tried to first analyze the high-resolution synchrotron powder diffraction pattern with all existing structures of similar compounds such as $M_2Si_5N_8$,[23] MSi_6N_8O,[24] and $MSi_2O_2N_2$,[14,15] and so forth, where M = Ca, Ba and Sr, but we hardly got any success in matching all the peaks of the diffraction pattern. Recently, a very similar phosphor system ($BaSi_3Al_3O_4N_5$) was synthesized and claimed to crystallize into a monoclinic structure in the $P2_1/m$ space group.[25] The powder XRD pattern of the Ba-based Unknown1 phase looked very similar to that of the $BaSi_3Al_3O_4N_5$ system in the low angular range (2θ = 5−65°), but an attempt of Lebail refinement using the $P2_1/m$ space group and Rietveld refinement with the position coordinates given in ref 25 for the entire 2θ range (2θ = 10−130°), a good match could not be obtained between the observed and the calculated data. The $BaSi_3Al_3O_4N_5$ structure did not seem to exist in the $P2_1/m$ space group, and the structural refinement in ref 25 seems to have been a mistake, because Si/Al tetrahedra with reasonable bond lengths has never been achieved using the atomic position data presented in ref 25. We thus implemented a series of structural determination processes, such as indexing, space group determination, profile matching, direct method, and Rietveld refinement, to identify the complete crystal structure of the Ba-based Unknown1 phase. The indexing of the diffraction pattern was performed using a TREOR program,[26] which was further checked with a DICVOL program[27] and EXPO 2009 software.[28] Before deciding the final results, every output of the TREOR program was verified by Lebail refinement. The Ba-based Unknown1 phase was found to crystallize into an orthorhombic lattice having the lattice parameters a = 9.48461(3) Å, b = 13.47194(6) Å, c = 5.77323(2) Å, and $\alpha = \beta = \gamma$ = 90°. The 2θ difference between the positions of observed and calculated peaks were less than 0.002° with a very good figure of merit (M(20) = 110 and F(20) =179). The indexing results revealed the extinction symbol $A\_a\_$, which gave rise to three different possible space groups (*Ama*2, $A2_1am$, and *Amam*). It was then subjected to a CheckGroup program embedded in the FullProf program[29] for exact space group determination. It became very difficult to decide the exact space group on the basis of the figure of merit obtained in this program, because it was identical for all three space groups. The exact space groups could not even be discriminated by subsequent Lebail refinement because the refinement converges with almost the same value of χ^2 and an identical fit between the observed and the calculated profile. The space group $A2_1am$ (no. 36) was thus chosen after extensive trial and error analysis and further confirmed by subsequent structural refinement (to be discussed later in this subsection). In addition to this phase, few peaks with very weak intensities corresponding to an impurity phase (α-Si_3N_4) were also present, which could be indexed with a trigonal structure in the $P31c$ space group having the lattice parameters a = 7.7463(6) Å, b = 7.7462(6) Å, c = 5.6170(7) Å, and $\alpha = \beta$ = 90° and γ = 120°. The peaks corresponding to the impurity phase, although very weak in intensity, were nonetheless very distinct and well separated from the peaks of the main phase. Hence, they could be easily excluded during the structural determination process.

The ensuing structural refinement revealed that the novel Ba-based Unknown1 phase was of type AB_5X_8 (A = Ba, B = Si and Al, X = O and N). Prior to discussion of the final structure determination process, it is necessary to mention an intriguing feature that we noticed during the course of the indexing and Lebail refinement. What we observed after a very fine interrogation of each and every peak in the diffraction pattern was that almost every peak in the diffraction pattern was split into two sets of peaks. The splitting was more prominent in the higher 2θ range as compared to the lower 2θ range. This result could not be understood clearly unless the structure was specified. The complete crystal structure and the stoichiometry, however, were determined using the direct method, simulated annealing, and Rietveld refinement. Thus, this result will be discussed in more detail later in this subsection. Due to this splitting, a compromised fit between the observed and the calculated profile with the relatively high value of χ^2 (>5) was obtained during Lebail refinement using only the single phase orthorhombic and impurity phase (α-Si_3N_4). It is worth mentioning here that the splitting in the peaks was apparent because the high resolution SR-XRD data were collected at a very fine step length (0.005°), and this splitting was barely discernible in the lab XRD data collected at step length (0.02°). In the lab XRD, the instrumental broadening is very effective in the determination of peak shape, and the peak separation due to the two phases was so small that they merged with each other and were not well resolved. Therefore, while analyzing the high resolution SR-XRD data, we first thought that the splitting might be due to the presence of some additional impurity phases, and we tried to match the unindexed peaks with the existing ICDD database, compared the diffraction pattern with similar compounds reported in the literature, and also indexed separately using the TREOR program. But none of the methods was helpful in indexing all the peaks present in the diffraction pattern even when considering the lower symmetry space groups that belong to monoclinic or triclinic systems.

dx.doi.org/10.1021/ja409865c | J. Am. Chem. Soc. 2014, 136, 2363−2373

The appearance of peak splitting for each of the individual peaks in the diffraction pattern suggests the presence of two identical phases having slightly different lattice parameters, which arose due to the process of chemical phase separation. This sort of phase separation was not surprising because it is often observed with inorganic materials. For example, in the single crystals of $Tl_{0.4}K_{0.4}Fe_{2-y}Se_{2-x}S_x$,[30] a phase separation into the $Tl_{0.4}K_{0.4}Fe_{2-y}Se_{2-x}S_x$-lattice (the S-poor phase) and the $Tl_{0.4}K_{0.4}Fe_{2-y}S_2$-lattice (the S-rich phase) at nanoscale has been observed with an increasing concentration of S doping. The powder XRD of $Tl_{0.4}K_{0.4}Fe_{2-y}Se_{2-x}S_x$ was completely refined with two sets of lattice constants: (1) a = 3.754 Å and c = 13.651 Å in the S-poor phase, and (2) a = 3.801 Å and c = 13.231 Å in the S-rich phase with the same space group ($I4/mmm$). A fine analysis of the SR-XRD pattern of Ba-based Unknown1 reveals that this system also behaves in a similar fashion as that of $Tl_{0.4}K_{0.4}Fe_{2-y}Se_{2-x}S_x$. The two identical phases of the Ba-based Unknown1 system are formed due to a chemical phase separation and to having the same AB_5X_8-type structure, but may consist of a different Si/Al ratio at the B site and subsequently a different O/N ratio at the X site of the structure. Extensive Rietveld analysis (discussed later in this subsection) revealed that the major phase consisted of a higher Si/Al ratio while the minor phase consisted of a lower Si/Al ratio. Both of the phases have identical crystal structures and space groups ($A2_1am$) but slightly different lattice parameters. A two phase Lebail refinement using a $A2_1am$ space group and slightly different lattice parameters (a = 9.48461(3) Å, b = 13.47194(6) Å, c = 5.77323(2) Å, $\alpha = \beta = \gamma = 90°$ for the major phase and a = 9.47791(4) Å, b = 13.45426(5) Å, c = 5.76940(2) Å, $\alpha = \beta = \gamma = 90°$ for the minor phase) resulted in an excellent match between the observed and the calculated profiles with a very low value of the χ^2 (= 1.7). To clearly depict the nature of peak splitting at the zoomed level, profile fits for some selected peaks are shown in Figure 5, and these are comprised of a low and high 2θ range obtained after the full pattern Lebail refinement using single phase and two phase orthorhombic structures, respectively, in the $A2_1am$ space group. It is evident from this figure that the peaks unaccounted for during single phase refinement were clearly accounted for during the two phase refinement giving rise to a very good fit between the observed and the calculated data with a nearly flat difference profile. The difference in the lattice parameters and the volume of the two systems was found to be very small, which indicated that the difference in the Si/Al ratio also would be very small. This argument was further verified by Rietveld refinement using a two phase mixture after the complete assignment of atomic positions using the direct method and simulated annealing. This type of phase separation might lead to poor thermal properties when the Ba-based Unknown1 was applied to the LED lighting.

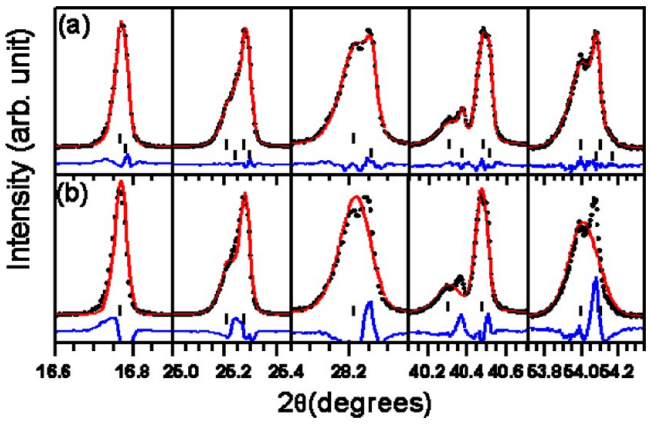

Figure 5. Observed (dots), calculated (red line), and difference (blue line) profiles for selected peaks obtained after full pattern Lebail refinement of the Ba-based Unknown1 phase using (a) two-phase orthorhombic structure in the $A2_1am$ space group and (b) single-phase orthorhombic structure in the $A2_1am$ space group. The vertical tick marks above the difference profile denotes the position of Bragg reflections for (a) the first major and second minor phase and (b) the first major phase only.

The ensuing direct method and simulated annealing process was implemented using the results of Lebail refinement for the major phase only and later the position coordinates so obtained were used as the initial model in the Rietveld refinement for both phases (major and minor). The exact atomic position of the heaviest ion, "Ba^{2+}", was first determined by a direct method using the G-Fourier program and was further confirmed using EXPO 2009 software[28] for an automatic structure solution. A simulated annealing optimization technique was used to determine the actual position of the other ions. After assigning the position of the heaviest ion (Ba ion), the structural determination process was first executed by excluding Al and O ions and considering only the Si ion as a cation and the N ion as an anion in the analysis, because it is very difficult to discriminate between Si and Al ions or O and N ions in the initial stage of refinement on the basis of powder XRD data due to their similar scattering factor.

Based on the results from the direct method and simulated annealing, Rietveld refinement using a Fullprof package[29] was finally carried out to determine the exact atomic positions of all the cations and anions. In the refinements, a pseudo-Voigt function and a linear interpolation between the set background points with refinable heights were used to define the profile shape and the background, respectively. Parameters, such as scale factor, zero correction, background, half-width parameters, the mixing parameters, lattice parameters, positional coordinates, and thermal parameters, were varied in the course of refinement. It was found necessary to use anisotropic peak broadening[31] in the refinements for SR-XRD. Rietveld refinement was first carried out only on the major phase by keeping the other phases in profile refinement (Lebail refinement) mode in order to obtain a better fit and more reliable position coordinates. After obtaining the atomic coordinates of the major phase, the same was used as an initial model for the second phase, and finally a complete Rietveld refinement was accomplished that considered all three phases (major phase, minor phase, and the α-Si_3N_4 phase). For the atomic coordinates of the α-Si_3N_4 phase, the coordinates given in ref 32 were used. Figure 6 shows a full pattern Rietveld refinement fit using a mixture of the three phases consisting of two orthorhombic phases in the $A2_1am$ space group and a α-Si_3N_4 phase in the $P31c$ space group. It is evident from this figure that a very good fit was obtained between the observed and the calculated profile with an almost flat difference profile and very good values for the agreement factors (R_p = 5.58, R_{wp} = 7.49, R_{exp} = 5.20, and χ^2 = 2.07). The quality of the Rietveld fit shown in Figure 6 clearly authenticates the reliability of the proposed structural model. The values of the structural parameters such as atomic position, thermal displacement, and the site occupancy factor obtained after the Rietveld refinement are listed in Table 2. It is noteworthy that, with "Ba"

dx.doi.org/10.1021/ja409865c | J. Am. Chem. Soc. 2014, 136, 2363−2373

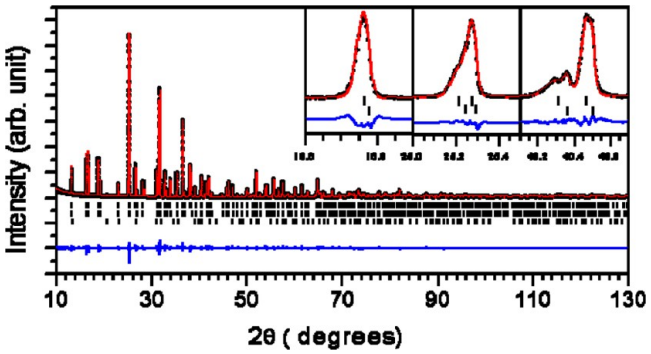

Figure 6. Observed (dots), calculated (red line), and difference (blue line) profiles obtained after the full-pattern Rietveld refinement of the major $BaAlSi_4O_3N_5$:Eu^{2+} and minor $BaAl_2Si_3O_4N_4$:Eu^{2+} phases using orthorhombic structure in the $A2_1am$ space group along with the impurity α-Si_3N_4 phase in the $P31c$ space group. Insets depict the zoomed portion of the Rietveld fit for some selected profiles (some of which are already shown for the Lebail refinement in Figure 5) to clearly depict the quality of the Rietveld fit at a zoomed level using a two-phase mixture. The vertical tick marks above the difference profile in the first, second, and third line from the top denote the position of Bragg reflections for the first (major), second (minor), and α-Si_3N_4 phases, respectively.

being the heaviest among all the ions, its thermal displacement parameter was found to be relatively larger than those of the O/N ion with respect to the isotropic thermal displacement parameters. This may have been due either to a disordered arrangement or to the anisotropic displacement of Ba ions in the crystal structure due to a certain amount of Eu^{2+} doping. Therefore, we considered the anisotropic thermal parameters for only the Ba ions in the Rietveld refinement, which resulted in acceptable values for all the thermal parameters of the cations and anions in the structure and significantly reduced the χ^2 value from 2.55 to 2.07. Although it is unconventional to employ the anisotropic thermal displacement parameters when using powder diffraction data, several cases[11,33] have made it necessary to consider anisotropic displacement parameters in order to achieve an acceptable quality of fit during structural refinement. The phase fractions obtained after Rietveld refinement were ∼77, ∼22, and ∼1% for the major phase, the second minor phase, and the impurity α-Si_3N_4 phase, respectively.

It is very difficult to determine the oxygen and nitrogen stoichiometry in the oxynitride compounds on the basis of X-ray diffraction techniques due their similar scattering factor, which also is the case for the Al and Si ions. Therefore, it becomes extremely difficult to specify the exact stoichiometry of these ions in order to specify an exact composition. This is why we gave the general formula "$Ba(Al,Si)_5(O,N)_8$:Eu^{2+}" for our novel phosphor, which signifies that some of the Si ion sites may also be shared by Al, and O ion by N . The only restriction placed on the number of these ions at the sharing sites is that that they should always maintain overall charge neutrality and a general formula of AB_5X_8 (A = Ba, B = Si and Al, X = O and N). Thus, this novel phosphor has an "AB_5X_8" (158)-type structure, which has never been reported so far and, thus, can be categorized as a Type IV phosphor (as described in Table 1). The stoichiometry of this novel phosphor, obtained after the Rietveld refinement, is found to be close to the stoichiometry of a synthesized phosphor; however, the exact Si/Al and N/O compositions need to be further verified using either high resolution neutron diffraction data or N/O combustion analysis. We would like to emphasize that irrespective of the Si/Al and N/O compositional variation, the overall structure of "158" will always be maintained.

Now the question arises, how it becomes possible to comment on the Si/Al and N/O ratios in the two identical structures when Al and Si ions (O and N ions) are indiscernible based on the X-ray diffraction data. Structural refinement

Table 2. List of Atomic Coordinates, Isotropic (U_{iso}) or Equivalent Isotropic (U_{eq}) Displacement Parameters, (Å^2) and Site Occupancy Factor (SOF) Obtained after the Full-Pattern Rietveld Refinement of $BaAlSi_4O_3N_5$:Eu^{2+} (first major phase) Using Powder SR-XRD Data

atom	Wyckoff site	*x*/*a*	*y*/*b*	*z*/*c*	U_{iso}/U_{eq} (Å^2)	SOF
Ba	4a	0.00000	−0.01227 (5)	0.00000	0.0240 (4)	1.00
Al1	4a	0.2453 (5)	0.46694 (15)	0.00000	0.0017 (6)	1.00
Si2	4a	0.0130 (5)	0.29205 (16)	0.00000	0.0024 (8)	1.00
Si3	8b	0.2319 (3)	0.16872 (12)	0.2524 (3)	0.0038 (4)	1.00
Si4	4a	0.4572 (4)	0.2842 (2)	0.00000	0.0082 (9)	1.00
O1	8b	0.2456 (8)	0.0409 (2)	0.2579 (6)	0.0141 (10)	1.00
N2	4a	0.0910 (9)	0.4054 (6)	0.00000	0.010 (3)	1.00
N3	4a	0.1318 (7)	0.2003 (6)	0.00000	0.004 (2)	1.00
N4	4a	0.1462 (6)	0.7097 (6)	0.00000	0.0040 (18)	1.00
N5	8b	0.4060 (5)	0.2152 (3)	0.2455 (8)	0.0019 (13)	1.00
O6	4a	0.3924 (8)	0.3971 (5)	0.00000	0.017 (2)	1.00
anisotropic displacement parameters (Å^2)						
atom	U^{11}	U^{22}	U^{33}	U^{12}	U^{13}	U^{23}
Ba	0.0157 (3)	0.0241 (4)	0.0321 (4)	−0.0141 (5)	0.0000	0.0000

compound name	$BaAlSi_4O_3N_5$:Eu^{2+}
wavelength (λ)	1.5472 Å
space group	$A2_1am$
space group no.	36
Z	4
lattice parameters	a = 9.48461(3) Å, b = 13.47194(6) Å, c = 5.77323(2) Å, $\alpha = \beta = \gamma = 90°$ (R_p = 5.58, R_{wp} = 7.49, R_{exp} = 5.20, and χ^2 = 2.07)

dx.doi.org/10.1021/ja409865c | J. Am. Chem. Soc. 2014, 136, 2363−2373

factors such as the atomic displacement parameters, the *R*-values, the χ^2, Durbin-Watson (DW) statistics parameter, and the overall fit of the profile pattern must be considered very carefully. A very close analysis of these factors in the output of the final refinement cycle provided sufficient information. However, these parameters were effective in the analysis once a good fit was obtained by considering only the Si and N ions (excluding Al and O ions) with all the parameters at their optimum values during the refinement. After a good fit was obtained by considering only the Si and N ions, one-by-one, we started replacing the Si ions with Al ions, and vice versa, by first concentrating on the value of the atomic displacement parameters (thermal parameter) of these ions, and thereafter by focusing on the *R* values and χ^2. We observed that the value of the thermal parameters changed dramatically with an incorrect assignment of ions, which in turn either reduced or increased the χ^2 and *R* values. In a similar manner, this process was repeated for O and N ions. This process was repeated with each and every individual ion until a very good fit with low *R*, χ^2, and acceptable values for all structural parameters were obtained. We tried all the available possibilities by even sharing the cation site with both Al and Si ions and some of the anion sites with both O and N while varying the occupancy (keeping the constraints of the occupancy). Another important factor that was taken into consideration was the assignment of Al/Si and O/N in such a manner that overall charge neutrality of the compound was always maintained along with the distribution of nitrogen and oxygen ions at available sites (i.e., triple site assigned conventionally by only N and bridging site by O and/or N). Thereafter, all the refinable parameters were left free during the refinement until acceptable values of the stoichiometry was obtained. We thus succeeded in getting a reasonable estimate of the stoichiometry after several cycles of structural refinement. The results of structural refinement revealed a chemical formula for the first major phase as $BaAlSi_4O_3N_5:Eu^{2+}$ and $BaAl_2Si_3O_4N_4:Eu^{2+}$ for the second minor phase. The summary of the structural parameters for the first major phase is listed in Table 2, and the second minor phase is provided in the Supporting Information. It is evident from these tables that the ratios of Si/Al and N/O oxygen are somewhat different in the major and minor phases, while the overall stoichiometry of "158" was maintained.

The structure of the $BaAlSi_4O_3N_5:Eu^{2+}$ phosphor obtained after the Rietveld refinement after considering all the facts discussed above and viewed along the [001] and [100] directions are shown in Figure 7a and b, respectively. It is evident from these figures that the structure is built up of a three-dimensional network of corner shared $(Al/Si)(O/N)_4$ tetrahedra in which half of the anion sites connect two neighboring Si ions (bridging site) and the other half connect three neighboring Si ions (triple site). Since the bridging site could be occupied by both O and N ions while the triple site preferably by the N ions, therefore, only N ions were assigned to all the triple sites in the structure, while the bridging sites were assigned to either O or N ions in an effort to maintain the overall charge neutrality and Wyckoff site restrictions. We also tried to assign both N and O ions to the bridging site, but it did not make a significant difference in the overall quality of fit. The Ba ions lay inside the hole created by the Si/Al−N/O tetrahedra network, and the Eu ions randomly occupied the sites of the Ba ions. The Si/Al−N/O bond lengths in the $(Al/Si)(O/N)_4$ tetrahedra obtained after the Rietveld analyses were found to lie in a range from 1.640(7) to 1.794(7) Å, which was

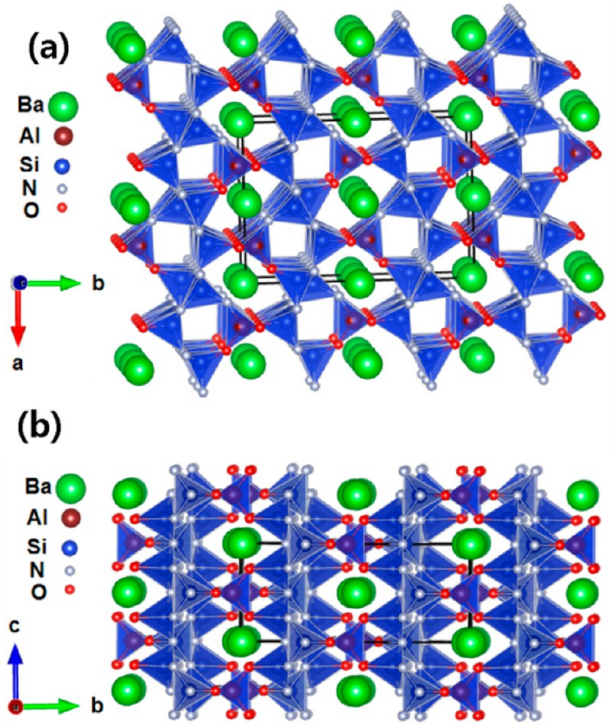

Figure 7. Crystal structure of $BaAlSi_4O_3N_5:Eu^{2+}$ viewed along (a) [001] and (b) [100] directions.

in very good agreement with the Si/Al−O/N ionic bond distances. The Al tetrahedrons acted as a bridging site between the alternate layers of the Si tetrahedra network. The structure looked very similar to the ring structure of $M_2Si_5N_8$ (258)[23] and $CaAlSiN_3$[34] phosphors, in which two M ions laid inside the hole created by the Si−N tetrahedra while only one Ba ion laid at the center of the hole in the present structure. Both these well-known phosphors had an orthorhombic structure, the former with a $Pmn2_1$ space group and the latter with a $Cmc2_1$ space group. The space group $A2_1am$ for the present phosphor and $Cmc2_1$ for the $CaAlSiN_3$ phosphor belonged to the same space group number with a difference only in the setting. Although the crystal system and the space group were identical with the $CaAlSiN_3$ system, the structure was entirely different with regards to the chemical formula and the lattice size. The "*b*" axis of the present phosphor was nearly double that of the "*b*" axis of $CaAlSiN_3$, while the "*a*" and "*c*" axes were almost of the same order. The structure of the second minor phase, with a fraction of only ∼22%, was found to be identical (AB_5X_8) to the major phase but with slightly different Si/Al and N/O ratios ($BaAl_2Si_3O_4N_4:Eu^{2+}$) and, therefore, was not discussed in great detail in the present investigation. In this structure, the charge neutrality conditions forced the assignment of all the available bridging sites by O ions only and the triple site by the N ions (the crystal structure figure is supplied in the Supporting Information).

The major phase of Sr-based Unknown1 was also found to be very similar to that of $Ba(Si,Al)_5(O,N)_8:Eu^{2+}$ with an orthorhombic structure in the $A2_1am$ space group and an identical atomic arrangement but with a slightly different lattice size (a = 9.35963(4) Å, b = 13.33688(6) Å, c = 5.73756(2) Å, $\alpha = \beta = \gamma = 90°$) due to a difference in the respective ionic radii. There was also another unknown impurity phase in the XRD pattern of Sr-based Unknown1. This impurity did not allow for

dx.doi.org/10.1021/ja409865c | J. Am. Chem. Soc. 2014, 136, 2363−2373

the fine refinement and led to a lower PL intensity, as shown in Figure 3. We skipped a further investigation of its structural refinement. However, a reasonable definition of the structure and stoichiometry for the Sr-based Unknown1 would be $Sr(Si,Al)_5(O,N)_8:Eu^{2+}$.

5. CONCLUSION

We discovered a new phosphor for use in LED applications, the formula of which was AB_5X_8 (A = Ba, B = Si and Al, X = O and N). This novel phosphor has an orthorhombic structure in the $A2_1am$ space group and emits a greenish blue light at near UV excitations. The structure of this novel phosphor is nonexistent in any of the inorganic compound databases, so that it definitely is a Type IV novel phosphor, which would never be called into question by any novelty arguments. The main purpose of the present investigation was not only to develop good phosphors to be used only in LED applications, but also to introduce our materials discovery strategy to as many scientists and engineers as possible. If the discovery strategy presented in the present investigation was adopted in some other materials discovery processes, more novel engineering materials could be discovered in a short period of time. Our strategy could be very useful in the area of alloy design for metals, cathode/anode materials for Li-ion batteries, fuel cell materials, structural ceramics, high Tc superconductor materials, multiferroic materials, and almost all inorganic-based functional materials.

■ ASSOCIATED CONTENT

Supporting Information

Brief description regarding the NSGACMS and PSOCMS processes and the definition of structural rank. The combinatorial compound library was tabulated, and the summary of the structural parameters for the second minor phase and the PSOCMS result for another unknown Type IV novel phosphor are also included. This material is available free of charge via the Internet at http://pubs.acs.org.

■ AUTHOR INFORMATION

Corresponding Author

kssohn@sejong.ac.kr

Author Contributions

†W.B.P. and S.P.S. contributed equally.

Notes

The authors declare no competing financial interest.

■ ACKNOWLEDGMENTS

This work was supported by the IT R&D program of MKE/IITA (2009-F-020-01) and partly supported by the National Research Foundation of Korea Grant funded by the Korean Government (NRF-2013R1A2A2A04015089).

■ REFERENCES

(1) Decker, S. LG Loses Round in U.S. LED Fight With Siemens Unit Osram. *Bloomberg*, Jul 10, **2012**; (http://www.bloomberg.com/news/2012-07-09/siemens-unit-osram-gets-mixed-ruling-in-lg-patent-fight-1-.html).

(2) Whitaker, T. Mitsubishi Chemical files LED-phosphor lawsuit against Intematix (Update). *LEDs MAGAZINE*, Dec 30, **2011**; (http://ledsmagazine.com/news/8/12/25).

(3) Seoul Central District Court finds Intematix and GVP infringe Mitsubishis red phosphor patent. *Mitsubishi Chemical Corporation News Release*, Feb 7, 2013; (http://www.m-kagaku.co.jp/english/newsreleases/2013/20130207-1.html)

(4) Park, W. B.; Shin, N.; hong, K.-P.; Pyo, M.; Sohn, K.-S. *Adv. Funct. Mater.* **2012**, *22*, 2258.

(5) Park, W. B.; Jeong, Y. S.; Singh, S. P.; Sohn, K.-S. *ECS J. Solid State Sci. Technol.* **2013**, *2*, R3100.

(6) Park, J. W.; Singh, S. P.; Sohn, K.-S. *J. Electrochem. Soc.* **2011**, *158*, J184.

(7) Yu, M.; Lin, J.; Fang, J. *Chem. Mater.* **2005**, *17*, 1783.

(8) Srinivas, N.; Deb, K. *Evol. Comput.* **1994**, *2*, 221.

(9) Kennedy, J.; Eberhart, R. *Proc. IEEE Int. Conf. Neural Networks* **1995**, *4*, 1942.

(10) Deb, K.; Pratap, A.; Agarwal, S.; Meyarivan, T. *IEEE Trans. Evol. Comput.* **2002**, *6*, 182.

(11) Park, W. B.; Singh, S. P.; Yoon, C.; Sohn, K.-S. *J. Mater. Chem. C.* **2013**, *1*, 1832.

(12) Park, W. B.; Singh, S. P.; Yoon, C.; Sohn, K.-S. *J. Mater. Chem.* **2012**, *22*, 14068.

(13) Park, W. B.; Singh, S. P.; Pyo, M.; Sohn, K.-S. *J. Mater. Chem.* **2011**, *21*, 5780.

(14) Zhu, W. H.; Wang, P. L.; Sun, W. Y.; Yan, D. S. *J. Mater. Sci. Lett.* **1994**, *13*, 560.

(15) Li, Y. Q.; Delsing, A. C. A.; De With, G.; Hintzen, H. T. *Chem. Mater.* **2005**, *17*, 3242.

(16) Seibald, M.; Rosenthal, T.; Oeckler, O.; Maak, C.; Tücks, A.; Schmidt, P. J.; Wiechert, D.; Schnick, W. *Chem. Mater.* **2013**, *25*, 1852.

(17) Allmann, R.; Hinek, R. *Acta Crystallogr., Sect. A: Found. Crystallogr.* **2007**, *63*, 412.

(18) Chiu, Y.-C.; Huang, C.-H.; Lee, T.-J.; Liu, W.-R.; Yeh, Y.-T.; Jang, S.-M.; Liu, R.-S. *Opt. Express* **2011**, *19*, A331.

(19) Wang, X.-M.; Wang, C.-H.; Kuang, X.-J.; Zou, R.-Q.; Wang, Y.-X.; Jing, X.-P. *Inorg. Chem.* **2012**, *51*, 3540.

(20) Mondal, P.; Jeffery, J. W. *Acta Crystallogr., Sect. B: Struct. Sci., Cryst. Eng. Mater.* **1975**, *31*, 689.

(21) Kahlenberg, V. *Cryst. Res. Technol.* **2001**, *36*, 319.

(22) Watanabe, H.; Wada, H.; Seki, K.; Itou, M.; Kijima, N. *J. Electrochem. Soc.* **2008**, *155*, F31.

(23) Schlieper, T.; Millus, W.; Schnick, W. *Z. Anorg. Allg. Chem.* **1995**, *621*, 1380.

(24) Stadler, F.; Kraut, R.; Oeckler, O.; Schmid, S.; Schnick, W. *Z. Anorg. Allg. Chem.* **2005**, *631*, 1773.

(25) Tang, J.-Y.; Xie, W.-J.; Huang, K.; Hao, L.-Y.; Xu, X.; Xie, R.-J. *Electrochem. Solid-State Lett.* **2011**, *14*, J45.

(26) Werner, P.-E.; Eriksson, L.; Westdahl, M. *J. Appl. Crystallogr.* **1985**, *18*, 367.

(27) Boultif, A.; Louer, D. *J. Appl. Crystallogr.* **1991**, *24*, 987.

(28) Altomare, A.; Camalli, M.; Cuocci, C.; Giacovazzo, C.; Moliterni, A.; Rizzi, R. *J. Appl. Crystallogr.* **2009**, *42*, 1197.

(29) Rodriguez-Carvajal, J. *FULLPROF*, Laboratory Leon Brillouin CEA-CNRSCEA/Saclay, 91191 Gif sur Yvette Cedex, France, Version May 2010.

(30) Feng, G.; Zuo, M.; Tan, S.; Xi, C.; Ling, L.; Zhang, L.; Tong, W.; Liu, H.; Yu, H.; Pi, L.; Zhang, C.; Zhang, Y. *Europhys. Lett.* **2012**, *100*, 47003.

(31) Stephens, P. W. *J. Appl. Crystallogr.* **1999**, *32*, 281.

(32) Toraya, H. *J. Appl. Crystallogr.* **2000**, *33*, 95.

(33) Clarke, S. J.; Chalker, P. R.; Holma, J.; Michie, C. W.; Puyet, M.; Rosseinsky, M. J. *J. Am. Chem. Soc.* **2002**, *124*, 3337.

(34) Piao, X.; Machida, K.-I.; Horikawa, T.; Hanzawa, H.; Shimomura, Y.; Kijima, N. *Chem. Mater.* **2007**, *19*, 4592.